Chapter 1 - Introduction

Materials Science is a field which seeks to understand the interrelationship between processing, properties, structure, and performance. This thesis will approach each of these cornerstones of the field through the study of metallic glasses. Due to their sensitivity to slow cooling rates, they offer distinct challenges in processing, while at the same time, they offer unique processing capabilities through technologies such as rapid discharge forming[1] and electromagnetic forming.[2] The properties of metallic glass are also their own unique set. Bulk metallic glasses (BMGs) have largely been treated as a one size-fits-all material. They can have high strength, large elastic limits, high hardness, high toughness, corrosion resistance, and a host of other commonly desirable traits, but all of these properties are not true for every alloy. The critical constraints of each application need to be considered individually. Saying metallic glasses are resistant to corrosion is like saying because titanium alloys are popular materials for aerospace applications, cadmium should be a good choice as well, because they both have a hexagonal closed packed crystal structure.

The first non-crystalline metallic alloys were discovered by Klement, Willens, and Duwez in 1960 during a series of experiments designed to probe the effects of extremely high cooling rates on the eutectic microstructure.[3] It was already known that as the cooling rate was increased, the interlaminar spacing would decrease.[4] Previous efforts in rapid cooling had been performed by propelling small droplets of molten alloy into another liquid. However, the cooling rate was limited by the vapor barrier which would be created by the molten droplet evaporating a liquid, as well as the need for the molten droplet to spread out rapidly into a thin layer to minimize the distance for heat to diffuse. Duwez was able to overcome both of these obstacles by dripping molten droplets onto a spinning copper wheel. The force from the wheel on the

droplet rapidly elongates it, and copper provides an optimal heat sink to rapidly draw heat away from the droplet.[5] Through this method, an Au-Si binary glass was formed.[3] Previously, the optimal technique for quenching molten metals was to allow droplets to fall into a viscous liquid to quench the molten droplet.

For almost a decade glasses were only able to be formed as either splats or thin ribbons. Even though this the melt spinning technique would eventually yield MetGlas, a commercially viable material, the field itself was limited by the thin casting limits.[6] Chen and Turnbull broke through this barrier by producing various alloys of the Pd-Si-Au/Ag/Cu family which were able to be cast to thicknesses greater than 1 mm.[7] Not until the developments of the Pd-Ni-Cu-P and Zr-Al-Ni-Cu alloys developed by the Inoue group at Tohoku University and the Zr-Ti-Be family of alloys developed by the Johnson group at Caltech were glassy alloys available in excess of a centimeter.[8–10]

With these new materials came a new wave of interest in metallic glass research. Now, more complicated geometries than simple ribbons could be created. These bulk glass formers lead to the initial commercial development of bulk metallic glasses. Products such as golf clubs and cell phone cases rapidly came to market. However, it was found that the lack of control during processing lead to impurities present in the final product which had devastating effects on the properties. Instead of being tough and strong, they were brittle.[11–13]

A fully amorphous MG's microstructure lacks grains, dislocations, or any of the other hallmarks of a traditional crystalline solid. Their microstructure is fairly simple. They can deform elastically up to their elastic limit, after which point they typically fail catastrophically due to a single shear band. So, taking cues from effective methods of toughing other metals, the thought was to extrinsically introduce second phases into the bulk metallic glass. Efforts were made with

the infiltration of powders,[14,15] fiber reinforcements,[16,17] sintering multiple glasses together,[18] extruding metallic glass powders with crystalline fibers,[19] and more.[20] An alternative approach is to partially crystallize the BMG upon cooling, which results in a multi-phase structure.[21] This led to the development of a new class of bulk metallic glass matrix composites, where a soft crystalline dendrite is grown to inhibit crack growth and increase toughness.

However, it wasn't until a study by Conner et. al.[22] that the cause for the increased toughness of metallic glass composites could be fully explained. It was discovered that if a metallic glass' thickness is, at most, twice the alloy's plastic zone size, then, in bending, ductility could be achieved. As a shear band grows from the outside of a bending surface, it will eventually reach the neutral axis of stress. At this point the tensile force will be zero, preventing the shear band from propagating any further. On the compressive side of the whisker, shear bands would not be able to propagate, since they are constrained by compressive stresses. By taking this result and expanding on it, an idea for a desired maximum length scale for a continuous amorphous matrix is apparent.

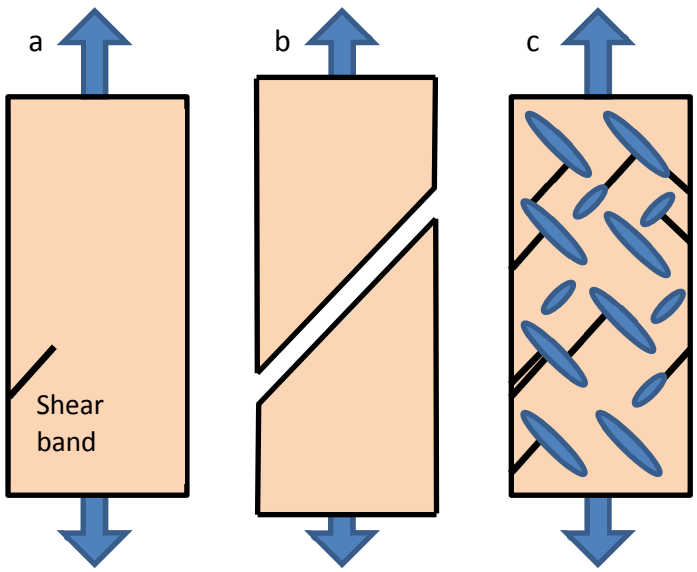

Figure 1-1: (a) A shear band beginning to grow in a BMG. (b) Failure by a single shear band in a bulk glass. (c) Multiple shear bands growth being arrested by a secondary phase.

If a second phase can be embedded in a BMG with this sort of spacing, ductility and increased toughness can be expected. Initially a shear band will nucleate and begin to grow. As long as it interacts with a second phase particle prior to becoming large enough to cavitate the shear band's growth will be arrested. At this point, the tip of the shear band will be blunted (the radius of curvature will go from extremely sharp to the size of the second phase particle). It is now energetically favorable to nucleate new shear bands instead of trying to propagate the initial one. For this reason, a well reinforced composite glass will exhibit superior plasticity (Figure 1-1).

The next step was to combine the idea of a BMG with a crystalline dendrite inside of it, along with controlling the spacing of the dendrite's arms to be approximately the critical shear band length. Hofmann et al.[23] were able to achieve this goal by holding molten ZrTiNbCuBe alloys below the liquidus temperature, but above the solidus. This technique allowed body centered cubic (bcc) dendrites to nucleate and grow. Previously, the composites had been rapidly quenched, and as such, the dendrite microstructure was heavily dependent upon the location within the sample and the apparent cooling rate. Dendrites nearest the surface experienced the fastest cooling, and wound up with very small dendrite morphologies. Those at the center had time for grain refinement, and wound up with more favorable mechanical properties, as their spacing was closer to the critical shear band length. Holding the entire ingot in the semisolid region allows dendrites to nucleate everywhere and grow at the same rate throughout. The whole sample can then be quenched, resulting in relatively uniform properties. Ductility was able to be achieved even in pure tension through this technique.[24]

The ability to hold a bulk metallic glass matrix composite (BMGMC) within the semi-solid region without causing rapid crystallization of an entire ingot upon rapid cooling offers different

processing techniques compared to a traditional BMG. One of the limitations of BMGs is their continual reliance on “beating the clock.” In other words, when processing a BMG one must always avoid crystallization. If a part requires multiple heating and cooling steps (such as forming feedstock ingots, then later heating and forging them into a final shape), crystallization must be avoided at all times. Even if the final part is to be sub-mm in thickness, if the feedstock ingot is thicker, then the critical casting thickness must be large enough for the feedstock to quench sufficiently. It must also not crystallize during heating prior to forging as well as after the forming process. On the other hand, if a BMGMC is being semisolidly processed,[25] the original ingot can be allowed to crystallize during cooling into feedstock. This is because during semisolid forging the ingot is reheated back above the solidus temperature. At this point, any crystals which have formed in the matrix will melt, leaving a mixture of liquid and equilibrium dendrite. The liquid can then readily be revitrified with a sufficient cooling rate.

Another class of BMGs containing crystals is those which partially crystallize in an uncontrolled manner upon quenching; these have been demonstrated in numerous studies.[26–29] A problem with this method is the inconsistency in properties of the final alloy, as well as the microstructure’s strong dependence upon the geometry of the final part. While an alloy may give an optimal microstructure for a 1 mm rod, when processed into a half millimeter thick sheet the dendrites may not have enough time to fully grow. Likewise, for a 2 mm thick rod the center may cool too slowly, and an excess of crystals could form. It may be a possibility to design an alloy around a particular application. First, determine the final geometry which will be used, then develop particular alloys for each situation. This method seems fairly difficult, however, as generally things are not of uniform thickness, and, even if they are, cooling rates may vary across a mold, giving different microstructures at different parts.

Since this thesis focuses predominantly on BMGs and BMCMCs, and each of these are heavily dependent upon both the thermodynamics of a system as well as the kinetics inside the system, it is informative basic theories of crystallization from a liquid. When a new crystalline phase, α, begins to form from a liquid, it will take up some volume of the liquid. It will also create a liquid/crystal interface. Both of these terms have an energetic cost, and if growth is assumed to be spherical, the resultant energy change in the system is

$$\Delta G = \left(4\pi r^2\right)\sigma_{sl} - \frac{4}{3}\pi r^3 \Delta G_V \tag{1}$$

where ΔG_V is the change in Gibbs free energy from the liquid to the crystal, σ_{sl} is the interfacial energy between the solid and liquid phases, and r is the radius of the nuclei. A system is at equilibrium when G is minimized. This minimum will be reached when the volume term becomes equivalent to the surface energy term. This can be found by taking $\left.\frac{\delta(\Delta G)}{\delta r}\right|_{r_c} = 0$,where r_c is the critical radius.

$$\begin{aligned} 8\pi r\sigma_{sl} - 4\pi r^2 \Delta G_V &= 0 \\ 4\pi r^2 \Delta G_V &= 8\pi r\sigma_{sl} \\ r &= \frac{2\sigma_{sl}}{\Delta G_V} \end{aligned} \tag{2}$$

This relationship can then be reinserted into our initial equation to find the critical free energy difference, ΔG_c

$$\Delta G_c = \frac{16\pi}{3}\left(\frac{\sigma_{sl}^3}{\Delta G_V^2}\right) \tag{3}$$

Another thought experiment which can be performed is estimating the amount of total fraction of volume taken up by spherical α nuclei as they grow in a liquid. Provided nucleation

occurs randomly and evenly throughout the liquid, and growth rate is constant and isotropic. For the first nuclei to form

$$V = \frac{4}{3}\pi r^3 = \frac{4}{3}\pi(vt)^3 \tag{4}$$

For any nuclei forming later, it would begin its growth at time τ,

$$V' = \frac{4}{3}\pi v^3 (t-\tau)^3 \tag{5}$$

For a given amount of time, $d\tau$, there will be $N d\tau$ nuclei forming. So, in the beginning of transformation (before particle impingement occurs) the total extended volume is

$$f_\alpha^e = \frac{4\pi}{3} N v^3 \int_0^t (t-\tau)^3 \, d\tau$$
$$f_\alpha^e = \frac{\pi}{3} N v^3 t^4 \tag{6}$$

As stated above, this will only be valid for very short times, or when *f* is small. In order to extend the theory to longer times, the overlap of nuclei forming inside existing nuclei which have already grown must be taken into account. For this reason, above, f_α^e is given as the fraction of volume which has been transformed, including multiple counting of areas due to overlapping nuclei. The actual volume transformed is related by

$$df_\alpha = df_\alpha^e f_L$$
$$df_\alpha = df_\alpha^e (1 - f_\alpha) \tag{7}$$

Rearranging , integrating, and solving for fraction transformed

$$\int \frac{1}{(1-f_\alpha)} df_\alpha = \int df_\alpha^e$$

$$\begin{aligned} \ln(1-f_\alpha) &= -f_\alpha^e \\ 1-f_\alpha &= \exp(-f_\alpha^e) \\ f_\alpha &= 1-\exp(-f_\alpha^e) \end{aligned} \tag{8}$$

Substituting back in the value for f_α^e from above

$$f_\alpha = 1-\exp\left(-\frac{\pi}{3}Nv^3t^4\right) \tag{9}$$

By grouping all of the constants on the right hand side together, a familiar result, the Johnson-Mehl-Avrami-Kolmogorov, is reached.

$$f_\alpha = 1-\exp(-Kt^n) \tag{10}$$

Where *K* is a collection of the nucleation rate, growth velocity, and geometric factors. By generalizing t^4 to t^n, different types of growth can be modeled. If desired, this equation can be further rewritten.

$$\begin{aligned} \ln(1-f_\alpha) &= -Kt^n \\ \ln[-\ln(1-f_\alpha)] &= \ln(Kt^n) \\ \ln[-\ln(1-f_\alpha)] &= \ln(K)+n\ln(t) \end{aligned} \tag{11}$$

By performing this simplification, plotting $\ln[-\ln(1-f_\alpha)]$ versus $\ln(t)$, the slope will give the resultant *n*. In the initial case, *n* = 4, and that could be seen as a particle growing in three dimensions, plus additional particles linearly being added to the system. In the cases of *n* = 1, 2, or 3 for transformations involving site saturation, it would indicate nucleation on surfaces, edges, and points, respectively.[30] In the third situation, growth could initially be seen as *n* = 4, but as soon as the point sites saturate, it changes to a value of 3. Likewise, if, instead of the α nuclei growing as spheres, they grew as circular platelets without saturated sites, it could be seen that *n* would also be equal to 3 for this case (with saturated point sites it would be 2).

To this point the temperature sensitivity of the nucleation and growth rates have not been discussed. While they will not be derived explicitly here, the nucleation rate can be found to be equal to[31]:

$$N = \frac{A}{\eta}\exp\left(-\frac{\Delta G_c}{k_b T}\right)$$

$$N = \frac{A}{\eta}\exp\left(-\frac{16\pi}{3}\frac{\sigma_{sl}^3}{k_b T(\Delta G_V)}\right) \quad (12)$$

Where k_b is Boltzmann's constant, A is comprised of constants, and η is the viscosity, whose temperature dependence can be given as

$$\eta(T) = \eta_0 \exp\left(\frac{DT}{T - T_0}\right) \quad (13)$$

The growth velocity can be expressed as

$$v = \frac{k_b}{3\pi L^2 \eta}\left[1 - \exp\left(-\frac{\phi(\Delta G_c)}{k_b T}\right)\right]$$

$$v = \frac{k_b}{3\pi\eta L^2}\left[1 - \exp\left(-\frac{16\pi}{3}\frac{\phi\sigma_{sl}^3}{k_b T(\Delta G_V)}\right)\right] \quad (14)$$

where ϕ is the average atomic volume and L is the average atomic diameter. By returning to Equation (9) above and inserting all of the expressions given, a full model can be given for the evolution of the microstructure of a material.

$$f_\alpha = 1 - \exp\left(-\frac{\pi}{3}\frac{A}{\eta}\exp\left(-\frac{16\pi}{3}\frac{\sigma_{sl}^3}{k_b T(\Delta G_V)}\right)\left(\frac{k_b}{3\pi\eta L^2}\left[1 - \exp\left(-\frac{16\pi}{3}\frac{\phi\sigma_{sl}^3}{k_b T(\Delta G_V)}\right)\right]\right)^{n-1} t^n\right) \quad (15)$$

$$f_\alpha = 1 - \exp\left[-\frac{Ak_b}{9\eta_0^2 e^{\frac{2DT}{T-T_0}} L^2} e^{\frac{16\pi}{3}\frac{\sigma_{sl}^3}{k_b T(\Delta G_V)}}\left(1 - e^{-\frac{16\pi}{3}\frac{\phi\sigma_{sl}^3}{k_b T(\Delta G_V)}}\right)^{n-1} t^n\right] \quad (16)$$

It is fairly evident that even this relatively simple model winds up with complicated behavior. The viscosity, growth velocity, and nucleation rate are all exponentially dependent upon temperature. As the temperature decreases the nucleation rate will grow quickly, and the growth velocity will also decrease rapidly. From this, we can see there will be a specific temperature at which the product of the nucleation and growth rates will reach a maximum, and this would be the temperature at which the growth of α would be fastest. In terms of forming a BMG, this is the critical temperature which must be rapidly cooled to in order to stand a chance at vitrification. Taking this as a way to think about the accidental composites, one can readily see how sensitive they can be to processing conditions. Indeed, casting a 2 mm rod from a copper mold will have different cooling conditions versus a copper mold. In this case, one may have the desired microstructure, while the other would not.

The following chapters will deal with a number of different methods, properties, processes, and new applications for metallic glasses and their composites. In this introduction, an outline has been made of the past history of metallic glasses, starting from their origins as a thin, difficult to process material to the development of bulk metallic glasses which are able to be cast in excess of one inch in thickness. The importance of designing metallic glasses such that their feature size is on the order of their plastic zone size is necessary in preventing catastrophic failure. Finally, the way to design composites to take advantage of this knowledge was discussed.

The second chapter is a study of how Charpy impact toughness can be affected by processing conditions. Various alloys are fabricated through suction casting, semi-solid forging, and commercially cast plates. Their performance is compared with that of traditional engineering alloys. A series of cryogenic Charpy tests of two BMGs, one BMGMC, and a well-

studied crystalline alloy are performed as well. In the end, a semi-solidly forged BMGMC has the highest impact toughness at room temperature and maintains parity with the well-performing BMGs even at cryogenic temperatures.

In the next chapter, the feasibility of joining bulk metallic glass matrix composites through rapid capacitive discharge is demonstrated. A series of measurements are performed to determine the maximum strength which can be achieved after welding, and it is found to be approximately that of the parent material. A cross section of the weld interface is inspected via SEM, and no traces of crystallization are found. The dendrite microstructure has not been heated sufficiently to be remelted nor heated long enough to coarsen. The matrix was able to be fully revitrified.

The fourth chapter explores the use of both bulk metallic glasses and bulk metallic glass matrix composites as energy absorbing materials in hypervelocity impacts. Flat sheets of Vitreloy 1 and an eggbox geometry of DH1 are impacted with a 3.17 mm aluminum sphere travelling at 2.7 km/sec. The eggbox's facets spread the ejected material out over a greater area, and are found to generate more light during the impact, implying a greater amount of energy was absorbed. The composite eggboxes are also welded into a multilayered Whipple shield, and they are able to fully stop the aluminum projectile with a velocity of 2.3 km/sec. The first two layers are penetrated, but the third stops any debris from passing through. The multilayered composites were found to outperform aluminum honeycomb sandwich panels for a given thickness. Metallic glasses and their composites are found to have a very promising future for hypervelocity impact protection, due to their high hardness and low melting point.

Next, preliminary measurements are performed to qualify metallic glasses as a potential material to become the replacement material for the gears on the Mars Space Laboratory. The

currently used Vascomax gears cannot suffer from high wear rates when operated at cryogenic temperatures. For this reason, Curiosity's gearboxes were outfitted with lubricants and heaters to prevent the gears from wearing excessively. Unfortunately, this requires substantial amounts of power and adds mass. Metallic glasses are reputed for their resistance to wear and are have been shown to lack a ductile to brittle phase transition,[32,33] so they should retain many of their attributes even at low temperatures.

A large series of metallic glass alloys are created and their wear loss is measured in a pin-on-disk test. Wear is found to vary dramatically among different metallic glasses, with some considerably outperforming Vascomax (most notably $Cu_{43}Zr_{43}Al_7Be_7$). Others, on the other hand, suffered extensive wear loss. Commercially available Vitreloy 1 was found to be much worse in wear compared to lab quality, likely due to impurities present during processing. This could explain some of the variability observed in the literature about this alloy. No conclusive correlations can be found between any set of mechanical properties (hardness, density, elastic, bulk, or shear modulus, Poisson's ratio, frictional force, and run in time) and wear loss. Heat treatments are performed on Vitreloy 1 and $Cu_{43}Zr_{43}Al_7Be_7$. Anneals near the glass transition temperature are found to possibly increase hardness slightly, but decrease wear loss significantly. Crystallization of both alloys leads to dramatic increases in wear resistance. Finally, wear tests are performed on the two alloys above. Vitreloy 1 experiences a dramatic decrease in wear loss, while $Cu_{43}Zr_{43}Al_7Be_7$ has a moderate increase. Meanwhile, gears are fabricated through three techniques: electrical discharge machining of 1 cm by 3 mm cylinders, semisolid forging, and copper mold suction casting. Initial testing finds the pin-on-disk test to be an accurate predictor of wear performance in gears.

The final chapter explores an exciting technique in the field of additive manufacturing. Laser engineered net shaping (LENS) is a method whereby small amounts of metallic powders are melted by a laser such that shapes and designs can be built layer by layer into a final part. The technique is extended to mixing different powders during melting, so that compositional gradients can be created across a manufactured part. Two compositional gradients are fabricated and characterized. Ti-6Al-4V to pure vanadium was chosen for its combination of high strength and light weight on one end, and high melting point on the other. It was inspected by cross-sectional x-ray diffraction, and only the anticipated phases were present. A 304L stainless steel to Invar 36 transitionary alloy was fabricated in both linear and radial gradients. It combines strength and weldability along with a zero coefficient of thermal expansion material. Only the austenite phase is found to be present via x-ray diffraction. Coefficient of thermal expansion is measured for four compositions, and is found to be tunable depending on composition.

References

(1) Johnson, W. L.; Kaltenboeck, G.; Demetriou, M. D.; Schramm, J. P.; Liu, X.; Samwer, K.; Kim, C. P.; Hofmann, D. C. Beating crystallization in glass-forming metals by millisecond heating and processing. *Science* **2011**, *332*, 828–33.

(2) Johnson, W. L.; Kltenboeck, G.; Demetriou, M. D.; Roberts, S.; Samwer, K.; Kaltenboeck, G.; Demetrious, M. Electromagnetic forming of metallic glasses using a capacitive discharge and magnetic field **2013**, *2*, 1–27.

(3) Klement, W.; Willens, R. H.; Duwez, P. Non-crystalline structure in Solidified Gold-Silicon Alloys. *Nature* **1960**, *187*, 869–870.

(4) Hultgren, R.; Olsen, W. T. Effect of rate of freezing on degree of segregation in alloys. *AIME Trans* **1950**, 1323.

(5) Duwez, P.; Willens, R. H.; Klement, W. Continuous Series of Metastable Solid Solutions in Silver-Copper Alloys. *J. Appl. Phys.* **1960**, *31*, 1136.

(6) Liebermann, H.; Graham, C. Production of amorphous alloy ribbons and effects of apparatus parameters on ribbon dimensions. *IEEE Trans. Magn.* **1976**, *12*, 921–923.

(7) Chen, H. .; Turnbull, D. Formation, stability and structure of palladium-silicon based alloy glasses. *Acta Metall.* **1969**, *17*, 1021–1031.

(8) Inoue, A.; Zhang, T.; Nishiyama, N.; Ohba, K.; Masumoto, T. Preparation of 16 mm diameter rod of amorphous Zr65Al7.5Ni10Cu17.5 alloy. *Mater. Transations, JIM* **1993**, *34*, 1234–1237.

(9) Peker, A.; Johnson, W. L. A highly processable metallic glass: Zr41.2Ti13.8Cu12.5Ni10.0Be22.5. **1993**, *63*, 2342–2344.

(10) Inoue, A.; Nishiyama, N.; Matsuda, T. Preparation of Bulk Glassy Pd40Ni10Cu30P20 Alloy of 40 mm in Diameter by Water Quenching. *Mater. Trans. - JIM* **1996**, *37*, 181–184.

(11) Gebert, A.; Eckert, J.; Schultz, L. Effect of oxygen on phase formation and thermal stability of slowly cooled Zr65Al7.5Cu17.5Ni10 metallic glass. *Acta Mater.* **1998**, *46*, 5475–5482.

(12) Liu, C. T.; Chisholm, M. F.; Miller, M. K. Oxygen impurity and microalloying effect in a Zr-based bulk metallic glass alloy. *Intermetallics* **2002**, *10*, 1105–1112.

(13) Conner, R. D.; Maire, R. E.; Johnson, W. L. Effect of oxygen concentration upon the ductility of amorphous Zr57Nb5Al10Cu15.4Ni12.6. *Mater. Sci. Eng. A* **2006**, *419*, 148–152.

(14) Zhu, Z.; Zhang, H.; Hu, Z.; Zhang, W.; Inoue, a. Ta-particulate reinforced Zr-based bulk metallic glass matrix composite with tensile plasticity. *Scr. Mater.* **2010**, *62*, 278–281.

(15) Conner, R. D.; Choi-Yim, H.; Johnson, W. L. Mechanical properties of Zr57Nb5Al10Cu15.4Ni12.6 metallic glass matrix particulate composites. *J. Mater. Res.* **2011**, *14*, 3292–3297.

(16) Conner, R. D.; Dandliker, R. B.; Johnson, W. L. Mechanical properties of tungsten and steel fiber reinforced Zr41.25Ti13.75Cu12.5Ni10Be22.5 metallic glass matrix composites. *Acta Mater.* **1998**, *46*, 6089–6102.

(17) Clausen, B.; Lee, S. Y.; Ustundag, E.; Aydiner, C. C.; Conner, R. D.; Bourke, M. Compressive yielding of tungsten fiber reinforced bulk metallic glass composites. *Scr. Mater.* **2003**, *49*, 123–128.

(18) Cho, S.-M.; Han, J.-H.; Lee, J.-K.; Kim, Y.-C. Fe-Based Nano-Structured Powder Reinforced Zr-Based Bulk Metallic Glass Composites by Powder Consolidation. *Korean J. Mater. Res.* **2009**, *19*, 504–509.

(19) Bae, D. H.; Lee, M. H.; Kim, D. H.; Sordelet, D. J. Plasticity in Ni59Zr20Ti16Si2Sn3 metallic glass matrix composites containing brass fibers synthesized by warm extrusion of powders. *Appl. Phys. Lett.* **2003**, *83*, 2312.

(20) Lee, K. S.; Kang, S.-H.; Lee, Y.-S. Synthesis of Zr-based bulk metallic glass–crystalline aluminum alloy composite by co-extrusion. *Mater. Lett.* **2010**, *64*, 129–132.

(21) Szuecs, F.; Kim, C. P.; Johnson, W. L. Mechanical Properties of Zr56.2Ti13.8Nb5.0Cu6.9Ni5.6Be12.5 Ductile Phase Reinforced Bulk Metallic Glass Composite. *Acta Mater.* **2001**, *49*, 1507–1513.

(22) Conner, R. D.; Li, Y.; Nix, W. D.; Johnson, W. L. Shear band spacing under bending of Zr-based metallic glass plates. *Acta Mater.* **2004**, *52*, 2429–2434.

(23) Hofmann, D. C.; Suh, J.-Y.; Wiest, A.; Duan, G.; Lind, M.-L.; Demetriou, M. D.; Johnson, W. L. Designing metallic glass matrix composites with high toughness and tensile ductility. *Nature* **2008**, *451*, 1085–9.

(24) Hofmann, D. C.; Suh, J.-Y.; Wiest, A.; Lind, M.-L.; Demetriou, M. D.; Johnson, W. L. Development of tough, low-density titanium-based bulk metallic glass matrix composites with tensile ductility. *Proc. Natl. Acad. Sci. U. S. A.* **2008**, *105*, 20136–40.

(25) Hofmann, D. C.; Kozachkov, H.; Khalifa, H. E.; Schramm, J. P.; Demetriou, M. D.; Vecchio, K. S.; Johnson, W. L. Semi-solid induction forging of metallic glass matrix composites. *JOM* **2009**, *61*, 11–17.

(26) Qin, C. L.; Zhang, W.; Asami, K.; Kimura, H.; Wang, X. M.; Inoue, A. A novel Cu-based BMG composite with high corrosion resistance and excellent mechanical properties. *Acta Mater.* **2006**, *54*, 3713–3719.

(27) Chang, H. J.; Yook, W.; Park, E. S.; Kyeong, J. S.; Kim, D. H. Synthesis of metallic glass composites using phase separation phenomena. *Acta Mater.* **2010**, *58*, 2483–2491.

(28) Lim, K. R.; Na, J. H.; Park, J. M.; Kim, W. T.; Kim, D. H. Enhancement of plasticity in Ti-based metallic glass matrix composites by controlling characteristic and volume fraction of primary phase. *J. Mater. Res.* **2010**, *25*, 2183–2191.

(29) Park, J. M.; Jayaraj, J.; Kim, D. H.; Mattern, N.; Wang, G.; Eckert, J. Tailoring of in situ Ti-based bulk glassy matrix composites with high mechanical performance. *Intermetallics* **2010**, *18*, 1908–1911.

(30) Cahn, J. W. Transformation kinetics during continuous cooling. *Acta Metall.* **1956**, *4*, 572–575.

(31) Schroers, J.; Wu, Y.; Busch, R.; Johnson, W. L. Transition from Nucleation Controlled to Growth Controlled Crystallization in Pd43Ni10Cu27P20 Melts. *Acta Mater.* **2001**, *49*, 2773–2781.

(32) Li, H.; Tao, K.; Fan, C.; Liaw, P. K.; Choo, H. Effect of temperature on mechanical behavior of Zr-based bulk metallic glasses. *Appl. Phys. Lett.* **2006**, *89*, 041921.

(33) Roberts, S.; Zachrisson, C.; Kozachkov, H.; Ullah, A.; Shapiro, A. a.; Johnson, W. L.; Hofmann, D. C. Cryogenic Charpy impact testing of metallic glass matrix composites. *Scr. Mater.* **2012**, *66*, 284–287.